ECS Transactions, 3 (8) 185-191 (2006)
10.1149/1.2356353, copyright The Electrochemical Society

Green Laser Crystallization of α-Si Films Using Preformed α-Si Lines

I. Brunets[a], J. Holleman[a], A.Y. Kovalgin[a],
A.A.I. Aarnink[a], A. Boogaard[a], P. Oesterlin[b], J. Schmitz[a]

[a] MESA+ Institute for Nanotechnology, Chair of Semiconductor Components,
University of Twente, P.O. Box 217, 7500 AE Enschede, The Netherlands.
[b] Innovavent GmbH, Bertha-von-Suttner-Str. 5, 37085 Goettingen, Germany.

In this work, amorphous silicon films with preformed α-Si lines were crystallized using a diode pumped solid state green laser irradiating at 532 nm. The possibility of controllable formation of grain boundaries was investigated. The crystallization processes in the rapidly melted silicon films were discussed. The influence of the crystallization parameters (i.e., energy density, scan velocity, etc.) and structure type (i.e., with and without preformed lines) on properties of the crystallized films was studied. The laser treatment with an energy density of 1.00 J/cm^2 at a laser pulse overlapping of 90% provided the optimal crystallization process with predefined grain boundary location. X-ray diffraction (XRD), SEM and AFM microscopy have been used to characterize the crystallized silicon films.

Introduction

Low thermal budgets are required to realize 3-D integrated circuits (IC) such as stacked memory devices (1, 2). Various integrated memory designs are investigated in (3-5). It is concluded that for a better performance of the circuit components, an additional quality improvement of low temperature silicon films is needed. Laser crystallization of low-temperature deposited amorphous silicon can provide polysilicon films at low substrate temperature, with sufficiently large grains (6-11). However, inherent to this technique is the random position of grain boundaries, leading to large device-to-device variations.

Recently, novel techniques were reported allowing the controlled formation of grain boundaries in a-Si laser crystallization through air-gap formation (12), two-pass laser crystallization (13), or the introduction of buried crystallization seeds (14). Bearing manufacturing cost and yield considerations in mind, it is at this time unclear what is the most effective solution for controlled grain formation.

In this paper, a novel approach for the controlled location of grain boundaries is described. The re-crystallization seeds are amorphous silicon strips fabricated with standard methods. The preformed α-Si lines patterned prior to the deposition of α-Si introduce an additional temperature gradient and provide controlled lateral crystallization of the molten material. This method can easily be introduced in silicon-compatible process flows and can allow a 3-D integration of devices with significantly improved characteristics.

The applied laser wavelength plays an important role during crystallization process. The glass substrates and interlayer oxide must be transparent at this wavelength to prevent their heating which can cause cracks and other damage or deformations. At the same time the absorption coefficient for amorphous Si film must be high enough to provide complete melting of the irradiated film. In case of excimer laser crystallization (308 nm

Downloaded 29 Jun 2009 to 130.89.112.86. Redistribution subject to ECS license or copyright; see http://www.ecsdl.org/terms_use.jsp

wavelength) the penetration depth is ≈ 10 nm (9), so primarily a thin top layer of silicon film is melted and only further thermal diffusion provides complete melting of the film. For this reason we chose for an irradiation at 532 nm wavelength, giving a lower absorption coefficient (15) leading to a more homogeneous melt (16). This increases the process window for re-crystallization in terms of the laser power and pulse duration.

Experimental

Silicon films with preformed α-Si lines

To realize a controllable crystallization of the amorphous silicon films we used preformed α-Si lines patterned prior to the deposition of the amorphous films (see Figure 1). First, a 50 nm thick α-Si film was deposited by LPCVD at 550 °C on top of a 0.7-μm thick thermally grown SiO_2 layer. After patterning the film, the lines with different width (from 0.4 up to 2.0 μm) were formed. Subsequently, a 100-nm thick α-Si layer was deposited using the same technique, which resulted in an amorphous film with a periodically varied thickness.

During the following laser crystallization, this varied film thickness influenced the temperature gradient in the lateral direction perpendicular to the laser scan direction. Re-crystallization will start where the temperature is lowest, and through this mechanism, the preformed lines determine where the main grain boundaries will occur.

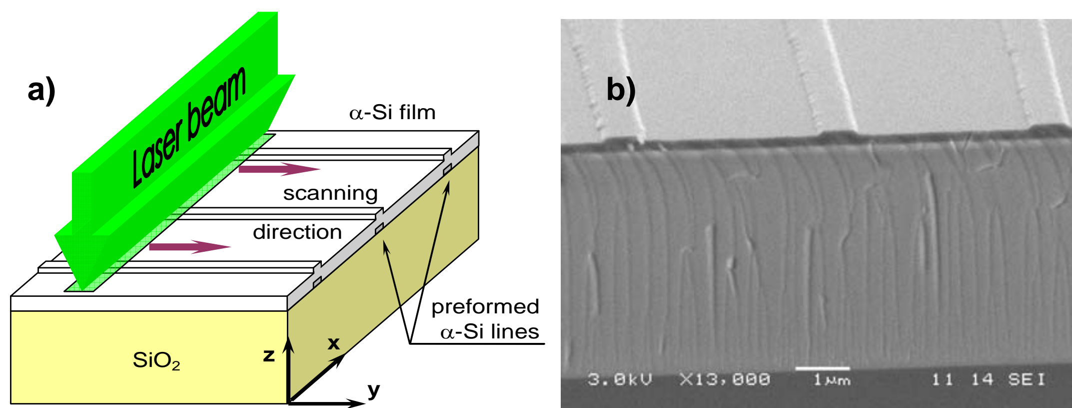

Figure 1. The laser crystallization process (a) and a cross-section SEM image of a silicon film with preformed lines (b).

Description of the laser system

In this work, the film crystallization was carried out using the laser optical system LAVA available at Innovavent GmbH. The system provided an up to 54 mm wide green laser beam (532 nm). A schematic block diagram of the optical system is shown in Figure 2. The laser system created a laser beam with a uniform top-hat profile along the x axis and a Gaussian profile along the y axis (see Figure 3). The beam's intensity profile was measured on the wafer plane using a beam profiling system equipped with a CCD camera, and a 40× microscope. The applied beam length was 5.15 mm and the width was 5.8 μm, both Full-Width Half-Maximum (FWHM) values. The average energy density in the beam was adjusted by an optical attenuator. The energy densities were calculated by dividing the total pulse energy by the FWHM area of the beam.

Downloaded 29 Jun 2009 to 130.89.112.86. Redistribution subject to ECS license or copyright; see http://www.ecsdl.org/terms_use.jsp

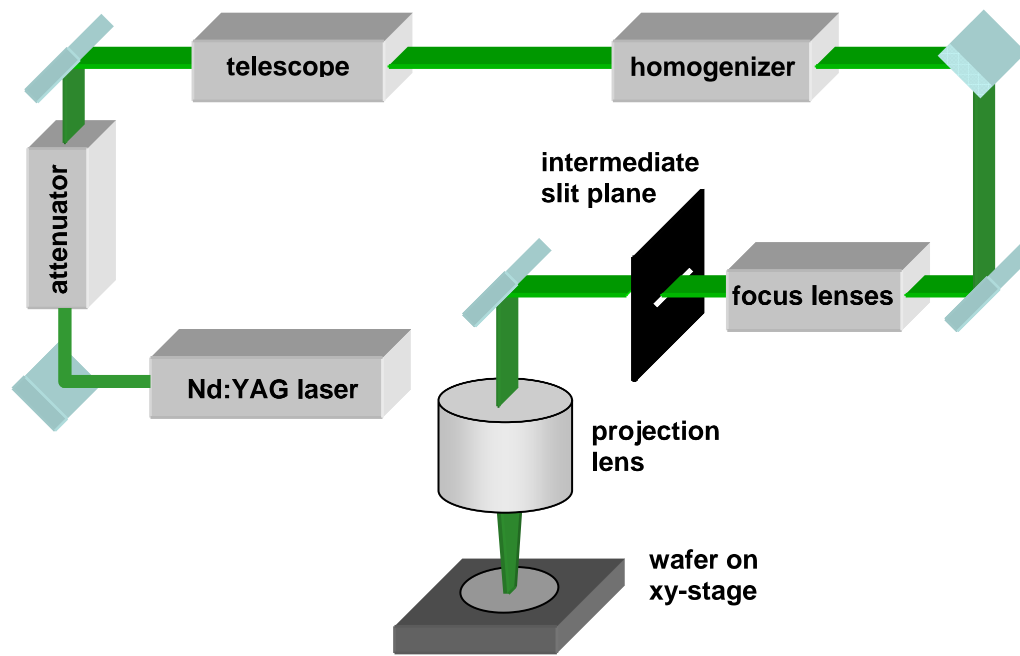

Figure 2. Block diagram of the optical system.

We used a frequency doubled Nd:YAG laser (model LDP-100MQG from Lee Laser) irradiating with an average power of 42.5 W at a repetition rate of 8.8 kHz. The pulse duration was 200 ns. The scan velocity was varied between 1 and 5 mm/second. To define and shape the line edges, an adjustable mechanical slit embedded in the intermediate slit plate was used. It was imaged on the wafer surface with a 10× demagnification.

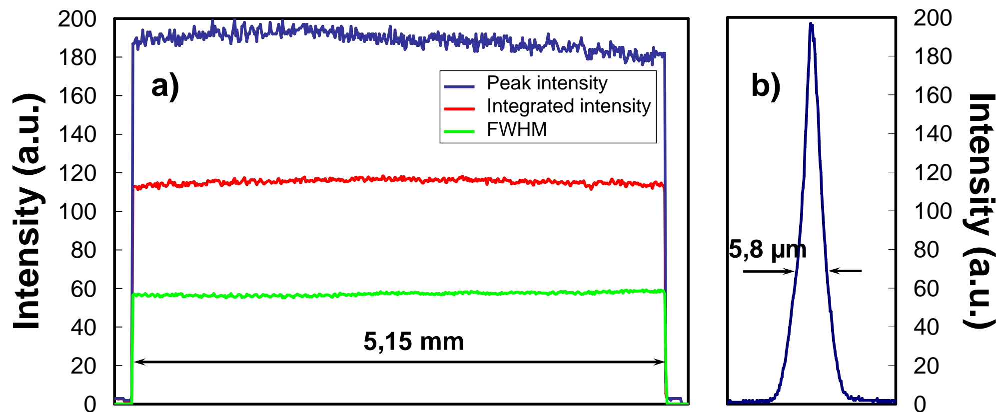

Figure 3. Laser beam intensity profiles: (a) along the x axis and (b) along the short y axis, see Figure 1 for details.

The wafer was located on a high accuracy motorized xy-stage. The projection lens was mounted on a high precision z-stage providing accurate focus adjustment. The depth of focus was ± 10 µm. The adjustment was done by making single pulse imprints on a test wafer followed by optical microscope inspection. The wafer stage, laser shutter and optical attenuator were computer controlled, so that the treatment steps with different

Downloaded 29 Jun 2009 to 130.89.112.86. Redistribution subject to ECS license or copyright; see http://www.ecsdl.org/terms_use.jsp

energy densities and pulse overlaps were done automatically, at different locations on the wafer.

Laser treatment of silicon films with preformed α-Si lines

The laser treatments of uniform silicon films and films with preformed α-Si lines were investigated and compared. For uniform films, the irradiated amorphous silicon film region was rapidly melted during a short laser pulse. After the pulse, the lateral crystallization process started at the interfaces between the solid and molten regions (13). The mentioned solid region was the polycrystalline silicon layer crystallized during the previous laser pulses. There were small crystallites with different orientations, serving as the seeds at the solid-liquid interface, where the crystallization of molten regions started. It was possible to obtain good quality films in the scanning direction (i.e., along the *y* axis) by optimizing the laser pulse length, energy density, beam overlapping, etc. However, the number of grain boundaries and, in general, the film quality in the perpendicular direction (along the *x* axis) was difficult to control (see Figure 4a). Due to the uncontrollable grain size, a dramatic device-to-device spread can be expected, caused by the random number and position of the grain boundaries localized in the device area. This problem is eliminated in a finely-grained crystalline film, but unfortunately such a film has poorer electrical properties and herewith impaired device functionality.

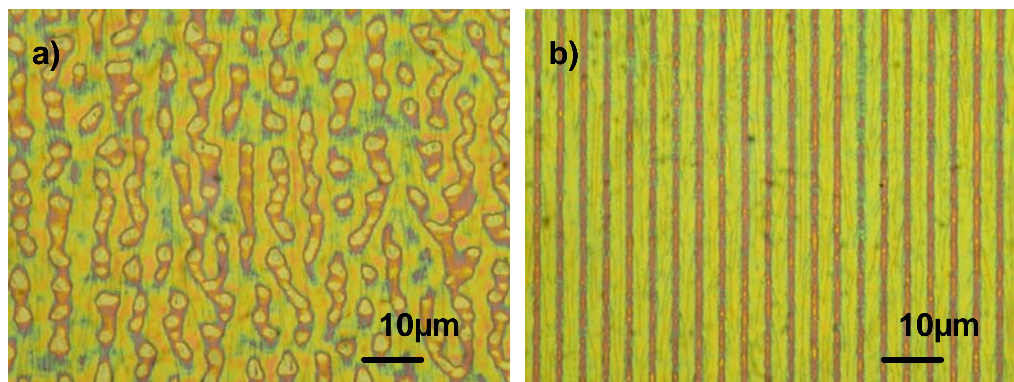

Figure 4. Typical optical-microscope surface images of crystallized Si films after Wright etching without (a) and with (b) preformed lines.

The crystallization process was improved by introducing the preformed lines prior to the deposition of amorphous silicon films. The addition of this extra process step resulted in a different crystallization behavior (see Figure 5). Although similar rapid melting occurred during the film irradiation, the interface between the solid and molten regions was not uniform and resembled that of a single amorphous layer. The periodically varied thickness locally resulted in non-molten regions deeply introduced into the molten silicon. These solid regions influenced the temperature gradient in the lateral direction perpendicular to the laser scan direction and served as the crystallization seeds where the super lateral crystal growth could initially start from (see Figure 5c-d). Thereby the dominate crystal orientation extend up to the grain boundaries with possible formation of the intragranular ridges and hillocks described in (17).

Downloaded 29 Jun 2009 to 130.89.112.86. Redistribution subject to ECS license or copyright; see http://www.ecsdl.org/terms_use.jsp

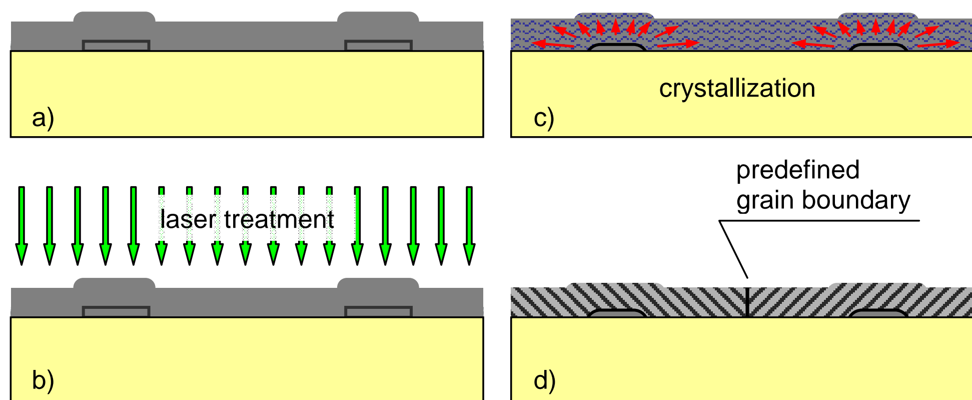

Figure 5. Crystallization process in silicon film with preformed lines (a) film formation, (b) laser treatment, melting of the silicon film, (c) crystallization process – super lateral growth, (d) final crystallized film with predefined grain boundary.

The average energy density and the area overlap for the subsequent laser pulses are critical parameters during crystallization process. The scan velocity is related to the laser pulse overlap (an overlap of 98% corresponds to a velocity of 1 mm/s, whereas an overlap of 90% corresponds to a velocity of 5 mm/s, both at 8.8 kHz repetition rate). The overlap area influences the crystallization mode, changing from lateral growth to homogeneous spontaneous nucleation in completely molten regions. During the lateral growth at the solid-liquid interface, the rest of liquid silicon is rapidly cooled and becomes a strongly undercooled liquid. Therefore the lateral crystal growth was stopped by homogeneous nucleation, formed a small-grained poly-Si region with poor electrical properties. Further re-crystallization with overlapping laser pulses was required, so the crystals created with one pulse are extended with the following one.

The laser treatment with an energy density of 1.00 J/cm^2, a laser pulse overlapping of 90% and repetition rate of 8.8 kHz provided the optimal crystallization process with predefined grain boundary location. Figure 4b shows the crystallized extremely long grains, visualized using Wright defect etching.

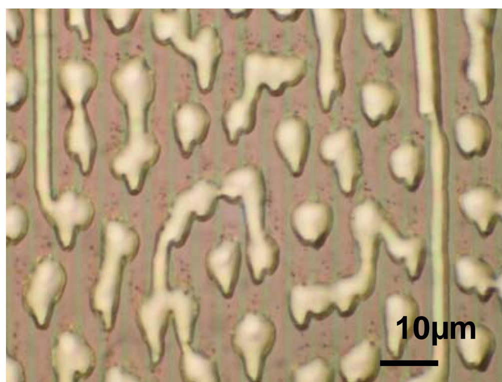

Figure 6. Optical image of silicon film agglomeration after laser treatment with a high energy density.

The irradiation with lower energies (< 0.6 J/cm^2 at 98% overlapping and < 0.8 J/cm^2 at 90% overlapping) resulted in partial melting of the film. For the lowest energy, only a

Downloaded 29 Jun 2009 to 130.89.112.86. Redistribution subject to ECS license or copyright; see http://www.ecsdl.org/terms_use.jsp

part of the film was crystallized. The energy densities higher than 1.0 J/cm^2 at 98% overlapping and 1.2 J/cm^2 at 90% overlapping lead to undesirable film heating. It was observed that the agglomeration of silicon and following crystallization of microcrystals give discontinuous and inhomogeneous films (see Figure 6).

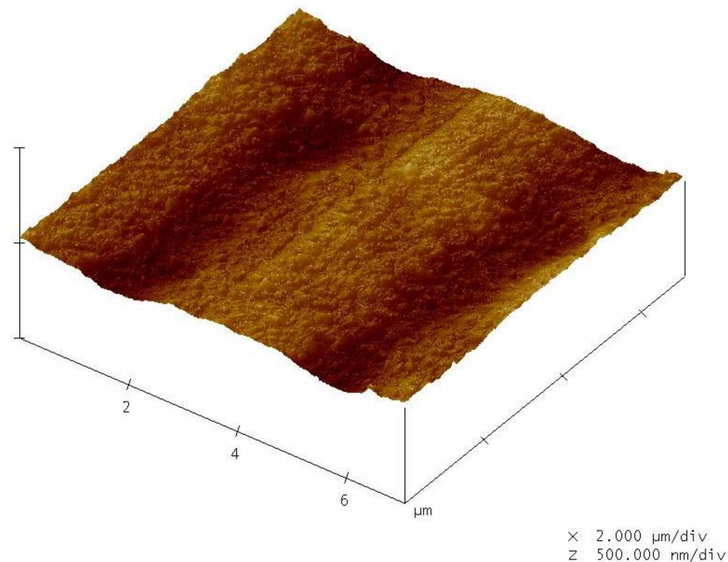

Figure 7. AFM image of crystallized Si film morphology (R_a = 19.9 nm, RMS = 24.2 nm).

As could be seen from analysis with optical microscopy (see Figure 4) and atomic force microscopy (see Figure 7), the surface of the silicon film even at optimum process conditions was not completely smoothed during laser crystallization. The crystallized film still exhibited a periodical height variation, remnant of the initial pre-formed lines. Therefore planarization (e.g. using chemical-mechanical polishing) is required before further device manufacturing.

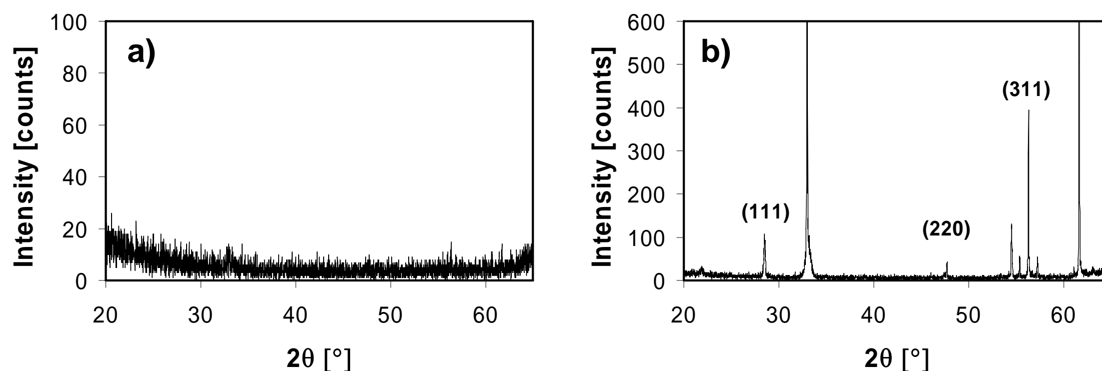

Figure 8. Measured XRD spectra (a) of 100 nm thick amorphous silicon film; (b) of crystallized silicon film with preformed lines. The XRD spectra were limited to 2θ = 65° to exclude the (100) peak of the silicon substrate.

XRD measurements of the crystallized silicon film with preformed lines (Figure 8b) show peaks indicating the presence of (111), (220) and (311) oriented grains. As a reference, the sample with 100 nm thick amorphous silicon film deposited by LPCVD at

Downloaded 29 Jun 2009 to 130.89.112.86. Redistribution subject to ECS license or copyright; see http://www.ecsdl.org/terms_use.jsp

550 °C on top of a 0.7-μm thick thermally grown SiO_2 layer was measured (Figure 8a). The shown measurement data confirmed the textured type of the laser-annealed silicon film.

Conclusions

Amorphous silicon films with underlying α-Si lines were deposited on thermally grown SiO_2. Laser crystallization with a green laser showed that the crystallization process is steered by the pre-patterned morphology. Through XRD analysis and optical inspection of the original, annealed and Wright-etched films, it was established that the films are indeed crystalline. Moreover, the grain boundary density was very low and the grain boundary position was controlled, allowing to design transistors in between grain boundaries.

Acknowledgments

This research was supported by the Dutch Technology Foundation (STW). Project number STW-TEL 6358.

References

1. K.C. Saraswat, S.J. Souri, V. Subramanian, A.R. Joshi, A.W. Wang, in *IEEE Int. SOI Conf.*, Proceedings p. 54 (1999).
2. S. Gu, et al., *J. Vac. Sci. Technol. B*, **23(5)**, 2184 (2005).
3. F. Li, X. Yang, A.T. Meeks, J.T. Shearer, K.Y. Le, *IEEE Trans. on Device and Material Reliability*, **4(3)**, 416 (2004).
4. S.B. Herner, et.al., *IEEE El. Dev. Lett.*, **25**, 271 (2004).
5. A.J. Walker, et al., in *2003 Symposium on VLSI Technology Digest of Technical Papers* (2003).
6. A.T. Voutsas, *Appl. Surf. Sci.*, **208-209**, 250 (2003).
7. S.D. Brotherton, D.J. McCulloch, J.B. Clegg, J.P. Gowers, *IEEE Trans. El. Dev.*, **40(2)**, 407 (1993).
8. S.-M. Han, M.-C. Lee, M.-Y. Shin, J.-H. Park, M.-K. Han, *Proc. of the IEEE*, **93(7)**, 1297 (2005).
9. P. Lengsfeld, N.H. Nickel, W. Fuhs, *Appl. Phys. Lett.*, **76(13)**, 1680 (2000).
10. M. Nerding, et al., *J. Appl. Phys.*, **91(3)**, 4125 (2002).
11. A. Hara, et al., *Jpn. J. Appl. Phys., Part 2*, **41(3B)**, L311 (2002).
12. C.-H. Kim, I.-H. Song, W.-J. Nam, and M.-K. Han, *IEEE El. Dev. Lett.*, **23**, 315 (2002).
13. L. Mariucci et al., *Thin Solid Films*, **383**, 39 (2001).
14. R. Ishihara, et al., *IEEE Trans. El. Dev.*, **51(3)**, 500 (2004).
15. G. Lubbert, B.C. Burkey, F. Moser, E.A. Trabka, *J. Appl. Phys.*, **52(11)**, 6870 (1981).
16. A. Hara, K. Yoshino, F. Takeuchi, N. Sasaki, *Jpn. J. Appl. Phys., Part 1*, **42(1)**, 23 (2003).
17. D.K. Fork, G.B. Anderson, J.B. Boyce, R.I. Johnson, P. Mei, *Appl. Phys. Lett.*, **68(15)**, 2138 (1996).

Downloaded 29 Jun 2009 to 130.89.112.86. Redistribution subject to ECS license or copyright; see http://www.ecsdl.org/terms_use.jsp